This article has been accepted for inclusion in a future issue of this journal. Content is final as presented, with the exception of pagination.

Hybrid and Passive Tissue-Anchoring Mechanism for Ingestible Resident Devices

Sanwei Liu, Sangwook Chu, *Member, IEEE*, Luke A. Beardslee, and Reza Ghodssi, *Fellow, IEEE*

***Abstract*— This work presents a hybrid tissue-anchoring mechanism that combines a pre-compressed microspring for autonomous actuation and a barbed microneedle (MN) for robust tissue anchoring with minimized preloading. The spring-microneedle unit (SMU) allows facile integration with potential ingestible resident systems to enable prolonged operation in the gastrointestinal (GI) tract (e.g. biomarker monitoring and therapeutic drug delivery). Utilizing high-precision direct laser writing (DLW), the SMU is directly fabricated on a flexible polyimide substrate, which that can be conveniently attached onto the exterior packages of ingestible devices to reduce the form factor and therefore to save room for multifunctional system components. The 3-D printed microspring can be compressed and embedded within a thin layer of dissolvable polymer (polyethylene glycol) and autonomously actuated with a ∼140-μm displacement upon polymer dissolution in aqueous media at 37°C. Mechanical calibration of the SMU demonstrated an average release force of 8 mN for a 100-μm actuation. According to our previous research into barbed MNs, this actuation force provides a large enough preload for a MN to achieve robust tissue-anchoring. Above all, the novel and effective tissue-anchoring mechanism has a great potential for enabling long-term operation of miniature biosensing and drug delivery systems. [2020-0169]**

***Index Terms*— Biomimetics, direct laser writing, ingestible devices, microneedles, tissue-anchoring.**

I. Introduction

MINIMALLY invasive, ingestible resident devices with prolonged GI operation offer significant opportunities to advance diagnostics and treatment of chronic GI symptoms [1]. For example, using an ingestible device to anchor a resident device on the GI mucosal surface can enable functionalities such as long-term monitoring and therapeutic administration to treat or mitigate inflammatory bowel disease (IBD) progression, which requires extended intervention [2], [3].

However, one key challenge in tissue anchoring is the development of a compact, passive mechanism that can be integrated into a pill-sized system. Existing tissue-anchoring technologies (e.g. chemical muco-adhesives and mechanical anchoring devices) require complicated systems and/or have a large form factor to provide effective preloading and control, limiting their ability to be integrated into ingestible devices [4]–[6]. Recently, the development of bio-inspired technology has provided insight for passive tissue anchoring using barbed MNs [7]–[10]. The barbed MN structures provide the advantage of a small tissue penetration force with a higher pull-out force, resulting in reduced preloading and robust tissue anchoring performance. However, their performances are limited by the resolution of conventional microfabrication methods and materials with the appropriate stiffness to achieve a high pull-out force to penetration force ratio (PPR).

Previously, we designed, fabricated, and demonstrated a parasite-inspired spiny MN (SMN) [11], closely mimicking the tissue anchoring proboscis of spiny headed worms [12]. Benefiting from high-fidelity direct laser writing (DLW) fabrication, the MN precisely replicates the biomimetic model with high-resolution features (ex. fine surface barb with tip diameter around 1 μm). The results demonstrate robust tissue anchoring performances on porcine small intestine tissues with a 25-mN pull-out force and more than an order of magnitude lower penetration force (1.6mN) [11], providing a simple and robust tissue-anchoring component with a PPR of over 10.

This work presents a passive, hybrid tissue-anchoring mechanism via incorporating micro-springs with barbed MNs within a compact structure, leveraging the state-of-the-art 3-D DLW technology to fabricate the hybrid structure on flexible substrates (Fig. 1). Specifically, each MN is built on top of a micro-spring that is compressed and constrained by a layer of dissolvable polymer. The spring-microneedle unit (SMU) can be actuated via the dissolution of polymer in aqueous media to release the MN for tissue anchoring.

Here, we successfully demonstrate the DLW fabrication of the SMU on a flexible polyimide surface and the compression of the SMU within dissolvable polyethylene glycol/PEG. We also demonstrate the efficacy of the polymer dissolution with DI water at body temperature (37°C) showing 140 μm of MN displacement within 103 mins. The SMU demonstrates good mechanical performance with a stable compression profile and an adequate release force capable of effective tissue anchoring. Additionally, we further investigate SMNs via characterizing the effect of Young's modulus and the surface microhook arrangement. The results provide an array of options for optimizing the tissue-anchoring performance to assist the future design of SMNs (e.g. tuning the preloading actuation force and tissue-anchoring strength). Above all,

Manuscript received May 14, 2020; revised May 27, 2020; accepted May 29, 2020. This work was supported by the National Science Foundation ECCS Program under Award 1738211. Subject Editor M. Rais-Zadeh. *(Corresponding author: Reza Ghodssi.)*

Sanwei Liu, Sangwook Chu, and Luke A. Beardslee are with the Institute for Systems Research, University of Maryland, College Park, MD 20742 USA (e-mail: swliu@umd.edu; swchu@umd.edu; labeardslee04@gmail.com).

Reza Ghodssi is with the Department of Electrical and Computer Engineering, University of Maryland, College Park, MD 20742 USA, also with the Fischell Department of Bioengineering, University of Maryland, College Park, MD 20742 USA, and also with the Institute for Systems Research, University of Maryland, College Park, MD 20742 USA (e-mail: ghodssi@umd.edu).

Color versions of one or more of the figures in this article are available online at http://ieeexplore.ieee.org.

Digital Object Identifier 10.1109/JMEMS.2020.2999448

1057-7157 © 2020 IEEE. Personal use is permitted, but republication/redistribution requires IEEE permission.
See https://www.ieee.org/publications/rights/index.html for more information.

Authorized licensed use limited to: University of Maryland College Park. Downloaded on June 14,2020 at 13:06:24 UTC from IEEE Xplore. Restrictions apply.

This article has been accepted for inclusion in a future issue of this journal. Content is final as presented, with the exception of pagination.

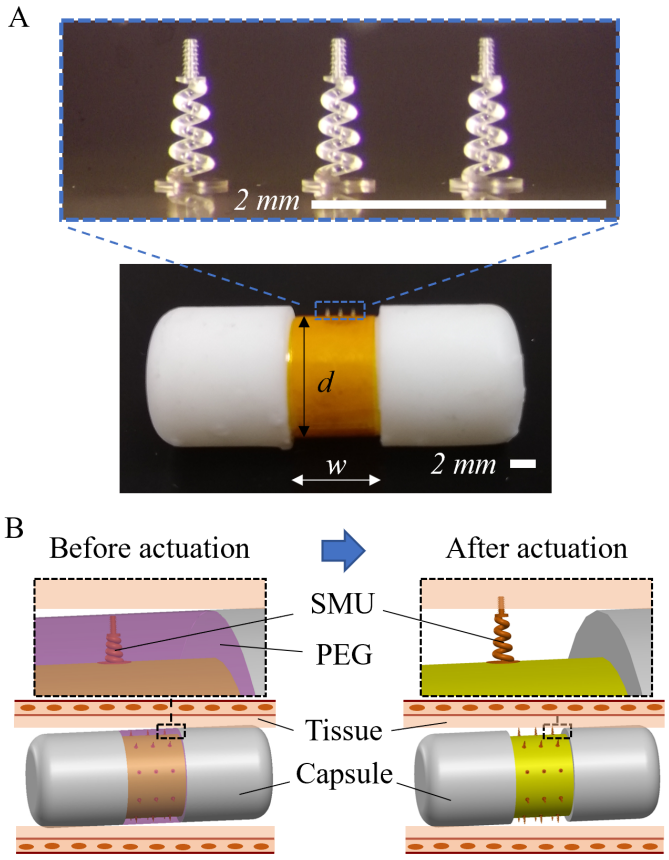

Fig. 1. Images of hybrid tissue-anchoring apparatus with (A) a 1 × 3 spring-microneedle unit (SMU) array wrapping around a pill-sized dummy capsule (d: 9.5 mm, w: 5 mm, scale bars: 2 mm), the zoomed-in image shows that each SMU consists of a barbed MN on top of a conical micro-spring. (B) Illustration of the tissue-anchoring mechanism with a compressed SMU (left) and released SMU (right) penetrating within the GI tissue, activated via PEG dissolution (4,000Mw, Sigma-Aldrich). The released SMU height (975 μm) is taller than the capsule trench (750 μm) so that the MN will be able to interact with the tissue when released.

the hybrid, compact, and passive mechanism provides great opportunities to address the challenges of deploying/anchoring ingestible resident devices in the GI tract.

II. Materials and Methods

A. Design of Hybrid Tissue-Anchoring Unit

Fig.1A shows a conceptual ingestible resident capsule integrated with a 1 × 3 SMU array compactly assembled on the surface trench (750 μm depth) of the capsule package using a flexible polyimide substrate (Kapton tape). Each MN is 260 μm tall with 48 barbs, allowing the robust tissue-anchoring performance demonstrated in the previous work. The backward facing barbs near the tip of the MN play an important role in enabling the low tissue penetration force and more than 10-fold higher pull-out force [11].

The conical micro-spring design allows reduced solid height for a compact design as each active coil is partially recessed within the next larger coil. The overall volume of the SMU is only about 5% of the overall capsule package volume. The conical design also provides lateral actuation stability as the base coils have larger diameters (250 μm to 100 μm) with less tendency to buckle than conventional compression springs. The design contains 4 spring coils with an 80-μm wire diameter, allowing stable directional actuation with an estimated spring constant of 340 N/m and 100 mN peak compression force at 300 μm displacement. These calculations are based on the conical spring model [12], as well as the measured Young's modulus and shear strength of the IP-S photoresist [14], [15]. The design parameters and calculations of the conical spring are listed in Table I.

TABLE I
Micro-Spring Design Characteristics

Symbol	Name	Value
H	Height	660 µm
d	Wire diameter	80 µm
N	Number of coils	4
$D1$	Base coil diameter	250 µm
$D2$	Top coil diameter	100 µm
E	Young's modulus	4.6 GPa [14]
τ_r	Shear strength	>180 MPa [15]
f_{max}	Maximum spring displacement or compression	300 µm
F_{max}	Peak compression force	100 mN
k	Spring stiffness	340 N/m
τ	Shear stress at f_{max}	158 MPa

The passive tissue-anchoring mechanism is depicted in Fig. 1B. Before actuation, the SMU array is compressed in solid PEG within the trench of the capsule (the overall SMU height is about 975 μm). After PEG dissolution in a 37°C aqueous environment (similar to the GI environment), the SMU array is actuated to anchor the MN tip into the GI tissue.

B. SEM Characterization

The SMU displays high-fidelity features with up to 1-μm resolution (Fig. 2). The conical spring demonstrates uniform spring wire diameter measured of 80 μm and an evenly distributed pitch of adjacent coils (Fig. 2A and Fig. 2B). The barbs on the MN surface are backward facing with sharp tips (Fig. 2C), which is essential for tissue anchoring [11]. The overall height of an uncompressed SMU is about 975 μm.

C. Direct Laser Writing Fabrication

The SMU is fabricated utilizing a high-precision DLW technology (Photonic Professional GT, Nanoscribe GmbH, Germany), which is based on highly localized interactions between a femtosecond laser and photosensitive material. First, the 3D model of the SMU is created via SolidWorks (Dassault System, France) computer-aided design (CAD) software. The CAD file, in the format of stereolithography (STL), is then imported and processed in the DeScribe software for fabrication coding. The design is then printed using the Dip-in Laser Lithography (DiLL) objective (25X magnification, NA = 0.8) with a negative-tone IP-S photoresist (Nanoscribe GmbH,

Authorized licensed use limited to: University of Maryland College Park. Downloaded on June 14,2020 at 13:06:24 UTC from IEEE Xplore. Restrictions apply.

This article has been accepted for inclusion in a future issue of this journal. Content is final as presented, with the exception of pagination.

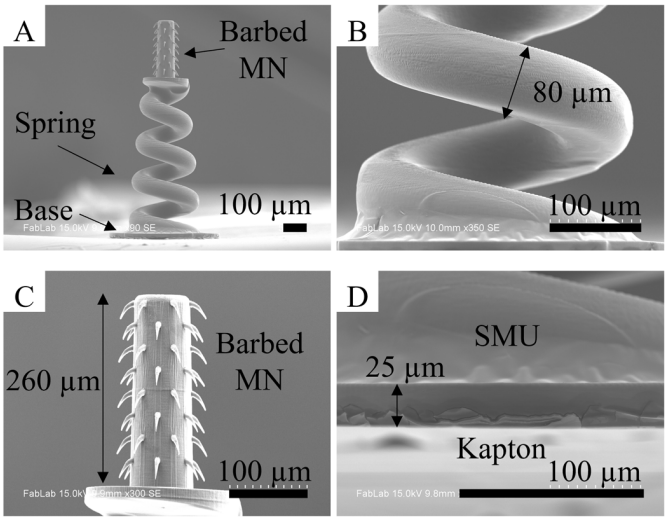

Fig. 2. SEM images of (A) SMU showing the conical spring (height; 660 μm) and barbed MN (height: 260 μm). (B) Base of the conical spring displaying uniform wire diameter. (C) MN with 8 rows of sharp, backward facing barbs arranged in rows of 6 barbs each. The MN base height is about 30 μm. (D) Intimate SMU/Kapton interface with base (height: 25 μm). The scale bars are 100 μm.

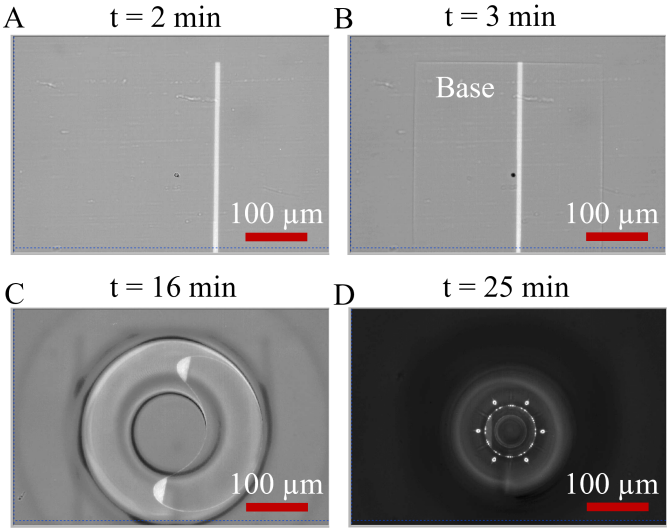

Fig. 3. Real-time images of the DLW process of a SMU. (A) t = 2 min, the laser interaction interface is within the Kapton tape, no photoresist is cured, (B) t = 3 min, the laser interaction interface is above the Kapton tape to create the SMU base, (C) t = 16 min, microspring fabrication within the central splitting block, and (D) t = 25 min, surface barbs fabrication showing the tips of the barbs are first cured as overhanging features (without any support). The illumination indicates the laser interaction region. Scale bars are 100 μm.

Germany, suitable for mesoscale prototyping compared to other photoresist and used by [10]) on Kapton tape on ITO-coated glass. The coded file is loaded into the DLW software, Nanowrite, for fabrication under the DLW settings of 50 mW laser power and 100 mm/s scan speed (galvo mode) to achieve 1-μm lateral slicing layer height, 1-μm hatching distance, and 26-minute fabrication time. After the laser writing, the sample is immersed in propylene glycol monomethyl ether acetate (PGMEA) to develop for 5 minutes, followed by 2-min of isopropyl alcohol (IPA) cleaning.

Fig. 3 shows the bottom-up DLW fabrication process of a single SMU on a Kapton tape covered ITO coated glass substrate. The base and conical spring are printed first, followed by the barbed MN structure. The transparency of Kapton tape allows the system to automatically locate the refractive interface on the ITO substrate surface. Therefore, the laser interaction is confined within the Kapton tape during the first 25 μm of printing and does not cure the photoresist. As a result, the as-fabricated SMU has a base thickness of about 25 μm instead of the designed value of 50 μm (Fig. 2D). This phenomenon of laser interaction can be observed in Fig. 3A (no photoresist is cured) and later Fig. 3B (the SMU base fabrication). Due to the limitation of the 300-μm by 300-μm lateral laser working area, the SMU is split into 5 parts to complete, with 2-μm crosslinking stitching overlapping. At t = 16 min, Fig. 3C shows that the microspring (250-μm base diameter, 80-μm wire diameter) sits within the central building block so that it is free from the risk of low connection strength at the overlapping region. At t = 25 min (Fig. 3D), the barb tips are first created without any support due to the bottom-up fabrication required to accommodate the microspring fabrication, which is notably different from the DLW process demonstrated previously for barbed MNs [11].

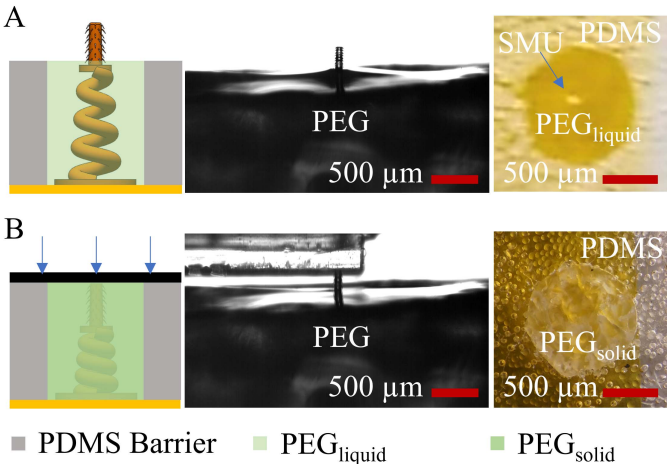

Fig. 4. Images showing the assembly of an embedded SMU (A) before and (B) after PEG solidification. The images are the (left) schematic, (center) side view, and (right) top view of the SMU-PDMS-PEG assembly setup. Scale bars are 500 μm.

D. SMU Compression and Assembly

Fig. 4 presents the assembly process for compressing an SMU with melted PEG. The selection of PEG is based on its melting point (53-58°C) and dissolution rate. The relatively low melting point allows the melted PEG at 100°C to have long enough transition time before solidification for assembly. The assembly process includes: 1) prepare a 2-mm by 2-mm, 750-μm thick PDMS film and pattern the film with a 1-mm biopsy punch to create a central hole, 2) place the PDMS well on the as-fabricated SMU substrate with the central hole and the SMU aligned concentrically, 3) add a droplet of aqueous PEG which is pre-melted at 100°C (Fig. 4A), and 4) immediately press the tip of the SMN completely into the

Authorized licensed use limited to: University of Maryland College Park. Downloaded on June 14,2020 at 13:06:24 UTC from IEEE Xplore. Restrictions apply.

This article has been accepted for inclusion in a future issue of this journal. Content is final as presented, with the exception of pagination.

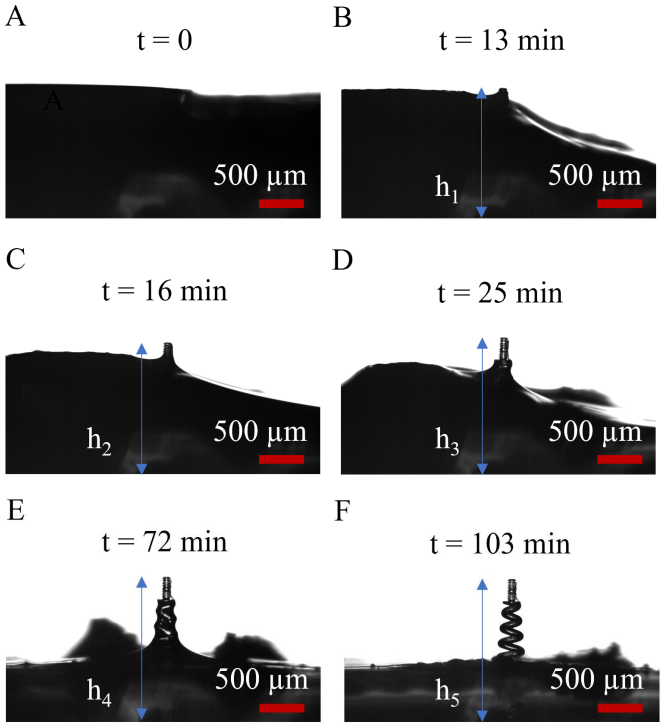

Fig. 5. Optical images showing the PEG dissolution process, revealing an embedded SMU with 37°C water. (A) t = 0 s, (B) t = 13 min, displacement measurement h_1 = 1.47 mm, the SMU tip appears, (C) t = 16 min, displacement measurement h_2 = 1.48 mm, (D) t = 25 min, displacement measurement h_3 = 1.56 mm. (E) t = 72 min, displacement measurement h_4 = 1.61 mm. (F) t = 103 min, displacement measurement h_5 = 1.61 mm. The recovery displacement is over 140 μm ($h_5 - h_1$). The images are taken by a high-speed camera (Redlake MotionPro HS-3, USA). Scale bars are 500 μm.

PDMS well and hold for 2 min so that the PEG will solidify and hold the compressed SMU in place (Fig. 4B). The SMU compression (225 μm) equals the height difference of the original SMU (975 mm) and the PDMS well (750 μm).

III. Results and Discussions

A. Polymer Dissolution Measurement

Fig. 5 displays the gradual dissolution of PEG upon rinsing with 37°C water (body temperature) to verify the passive SMU actuation mechanism. Initially, the SMU is embedded in PEG after assembly (Fig. 5A). As body temperature (38°C) water droplets (~0.06 μL) are gradually added onto the assembly, the SMU tip slowly appears with a measured height from the base (including the substrate and the SMU) of 1.47 mm (h_1) and 1.48 mm (h_2) at t = 13 min (Fig. 5B) and t = 16 min (Fig. 5C), respectively. At t = 25 min, the entire MN appears with a measured height of 1.56 mm (h_3) (Fig. 5D). At t = 72 min, the majority of the SMU appears with some PEG and trapped within the space of the microspring with a measured height of 1.61 mm (h_4) (Fig. 5E). At t = 103 min, the majority of the SMU appears and the final height remains at 1.61 mm (h_5) (Fig. 5F). Because the initial displacement at t = 0 cannot be directly measured (the microneedle is not visible when fully embedded in the PEG), the estimated minimum displacement recovery is 140 μm, determined via

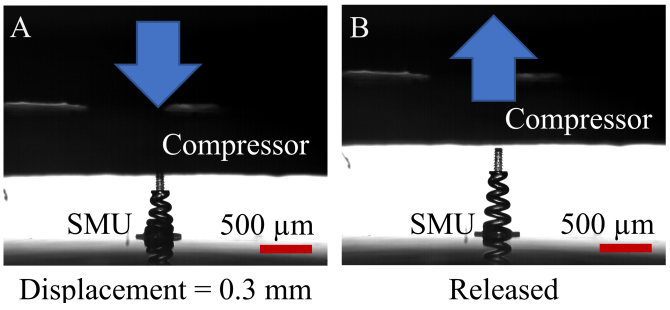

Fig. 6. Characterization of the mechanical compression and release of the SMU showing that the spring can withstand a 300-μm compression displacement and fully recover after release. Scale bars are 500 μm.

subtracting the displacement between h_5 and h_1. This measured actuation displacement is large enough for the MN to interact with GI tissue, confirming the autonomous actuation capability. Note that the dissolution time for the maximum actuation can be tuned by altering the molecular weight of the selected PEG (the higher molecular weight, the slower dissolution) [15]. Future work includes demonstrating a faster dissolving mechanism to allow MNs to penetrate the tissue before the capsule to be pushed away. Additionally, the design of the polymer coating allows the future design of targeted actuation of the MNs based on the media pH profile capable of targeting specific GI locations (ex. the stomach has low pH while the small intestines have neutral pH) [16].

B. SMU Actuation Measurement

The fabricated conical micro-spring requires mechanical characterization to verify stability and compression failure. Fig. 6 presents the typical compression and release profile of the SMU showing that the spring can withstand a 300-μm compression displacement and fully recover after release. There was no spring coil damage observed during the test. Also, the SMU remains adhered to the polyimide substrate during the test. The results indicate that the design characteristics are appropriate for the SMU actuation.

The SMU is also quantitively tested using a universal testing machine (Model 5565, Instron, MA, USA) with tensile and compressive modes containing a +/−50 N load cell and 3D-printed fixture assembled to the upper sensing column to compress the SMU samples. During the test, an SMU is placed under the movable sensing column of the tester. After balancing the load cell, the upper movable column moves towards and pushes the SMU with its fixture at the speed of 0.05 mm/s until the compression displacement reaches 300 μm. After the compression, the upper column moves upwards to release the SMU at the same speed. Throughout the test, the upper sensing column records time, displacement, and force measurement. This process is video recorded using a stereomicroscope (Leica M125, Germany) and a digital camera (Sony α6000, Japan).

Fig. 7A presents a typical compression and release force measurement profile of an SMU, showing that the compressional force increases as the displacement increases. Before releasing, the compression force decreases from

Authorized licensed use limited to: University of Maryland College Park. Downloaded on June 14,2020 at 13:06:24 UTC from IEEE Xplore. Restrictions apply.

This article has been accepted for inclusion in a future issue of this journal. Content is final as presented, with the exception of pagination.

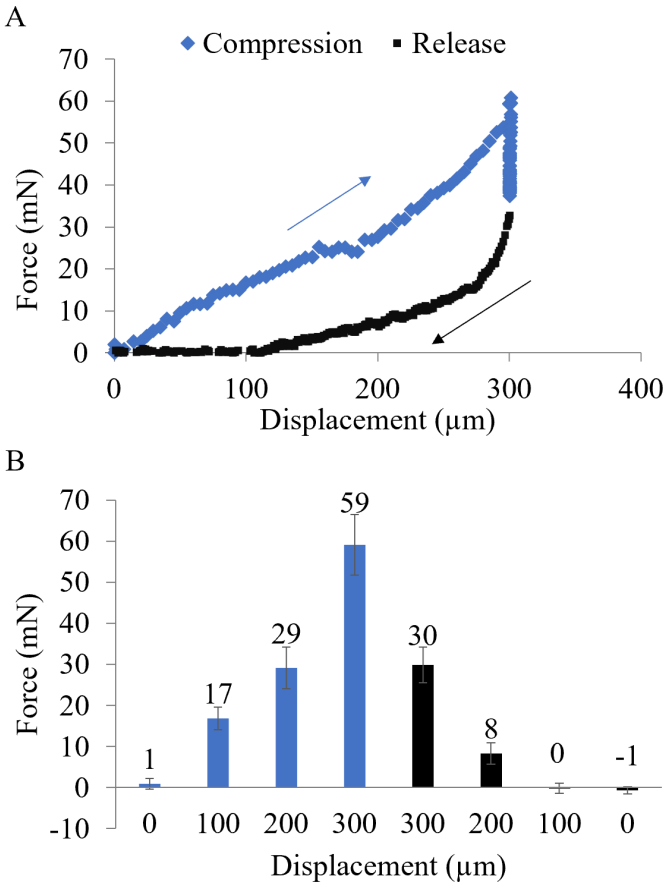

Fig. 7. Mechanical characterization of SMU during compression and release showing (A) a representative force-displacement curve, and (B) average force measured at every 0.1mm displacement (N = 5). The loading rates are 3mm/min and 0.6mm/min for compression and release, respectively, to mimic the PEG assembly and dissolution rates.

59.3 mN to 32.7 mN, indicating stress relaxation. The difference between the compression and release (hysteresis) indicates that the SMU spring has a considerably large energy dissipation, possibly due to the internal friction of the building block material (IP-S, Nanoscribe Gmbh, Germany). The hold time of the compression of the SMUs are about 30s. Future work needs to address the total relaxation of the SMU to demonstrate long-term actuation performance.

Fig. 7B shows that the average compression force increases up to 59 mN over a 300-μm displacement, showing an average spring constant of 197 mN/mm. The lower calibration values compared to the analytical estimations are attributed to the variation in the mechanical property of the cured photoresist (IP-S, Nanoscribe Gmbh, Germany). The releasing force, measured after stress relaxation, demonstrates 8 mN at 100-μm SMU actuation relative to the maximally compressed state (equivalent to a 200-μm displacement from its position before loading), ultimately indicating sufficient mechanical rigidity to withstand the 1.6mN MN penetration force [11] and the 8μN peristaltic force [18]". Additionally, cyclical mechanical tests of both single SMU and 1 × 3 SMU array are presented in Table II and Table III, respectively. The measured recovery force at 200 μm displacement or 100 μm

TABLE II
REPRESENTATIVE SINGLE SMU CYCLIC PERFORMANCE

Cycle	Force at 300 μm displacement (mN)	Force at 200 μm displacement or 100 μm actuation (mN)
Cycle 1	67	8
Cycle 2	42	4
Cycle 3	32	3
Cycle 4	29	2
Cycle 5	28	3

TABLE III
REPRESENTATIVE 1 × 3 SMU ARRAY CYCLIC PERFORMANCE

Cycle	Force at 300 μm displacement (mN)	Force at 200 μm displacement or 100 μm actuation (mN)
Cycle 1	132	40
Cycle 2	126	37
Cycle 3	121	31
Cycle 4	116	30
Cycle 5	132	40

actuation demonstrated a large enough actuation force for robust tissue anchoring (>2 mN per MN). Notably, the 1 × 3 SMU array presents a much higher actuation force, possibly due to secondary parasitic motions of individual SMUs (e.g. lateral collapse) that provide interactive supports to each other, demonstrating the advantage of an SMU array for future capsule integration.

C. MN Characterization

Our previous study of the bio-inspired, tissue-anchoring MNs demonstrated exceptionally low tissue penetration forces while maintaining high pull-out forces [11], with an over 10-fold enhancement in pull-out/penetration performance compared to the state-of-the-art [7]–[9]. Here, we further investigated the photoresist material properties and the spiny microhook patterns to guide the future design of the SMU to adjust the actuation force and tissue-anchoring strength.

Fig. 8 presents the effect of presence of the microhooks, needle material, hook base diameter, and microhook pattern density on tissue anchoring performance by comparing the pristine SMN design to barbless microneedles, microneedles printed with a softer photoresist material, microneedles equipped with larger microhooks, and microneedles with fewer microhooks.

The microneedle with no surface microhooks (Type I) relies solely on the frictional force between the needle surface and the surrounding tissue in this anchoring process, and as a result, there is no significant difference between the penetration and pull-out forces with both measuring low force levels. SMNs fabricated with softer photoresist (Type II) provide less effective anchoring (>4-fold lower pull-out force) compared to the pristine SMN (Type III), indicating the importance of material stiffness (Young's modulus: 1 GPa vs. 4.6 GPa, [14]) in achieving robust mechanical interlocking between the microhooks and the intestinal tissue.

Authorized licensed use limited to: University of Maryland College Park. Downloaded on June 14,2020 at 13:06:24 UTC from IEEE Xplore. Restrictions apply.

This article has been accepted for inclusion in a future issue of this journal. Content is final as presented, with the exception of pagination.

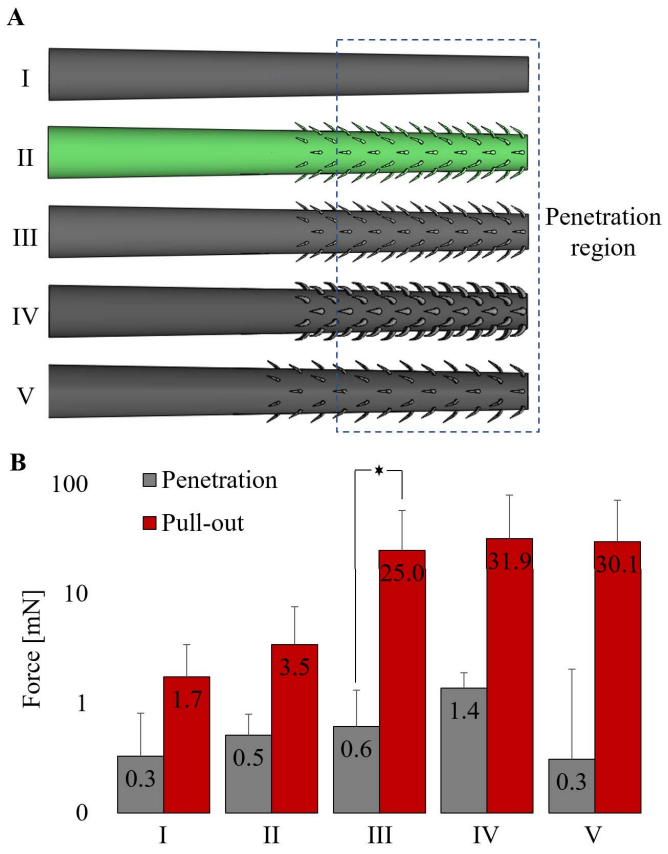

Fig. 8. (A) Schematics of five different microneedles tested with 0.4 mm penetration displacement: (I) Spine-less microneedle made of IP-S photoresist (IP-S, no hook, E = 4.6 GPa, microhook base diameter = 8 μm, axial spacing = 60 μm, n = 4); (II) SMN made of Ormocomp photoresist (soft microhooks, E = 1 GPa, microhook base diameter = 8 μm, axial spacing = 60 μm, n = 4); (III) Pristine SMN (IP-S, E = 4.6 GPa, microhook base diameter = 8 μm, axial spacing = 60 μm, n = 17, $*$ P < 0.05, one-way ANOVA); (IV) SMN (IP-S, E = 4.6 GPa, 2X large microhook base diameter = 16 μm, axial spacing = 60 μm, n = 5); (V) SMN (IP-S, E = 4.6 GPa, microhook base diameter = 8 μm, less microhooks with 1.5X axial spacing = 90 μm, n = 4). (B) Comparisons of penetration forces at 0.4 mm displacement and maximum pull-out force for the five different microneedles, loading rate at 0.01 mm/s.

These findings are consistent with the evolutionary success of the spiny headed worm's effective parasitic tissue anchoring structure (sclerotized surface hooks). Additionally, SMNs with a doubled hook base diameter (Type IV), showed only a slight increase in pull-out force while the penetration force showed a 2-fold increase compared to the pristine SMN. Note that the hook tip diameter is the same as the pristine SMN (1 μm) and the needle trunk dimensions remains the same. This suggests that increasing the hook size brings marginal improvement to the strength of tissue anchoring while the increased contact area of the larger microhooks leads to greater penetration resistance, ultimately resulting in a lower PPR. On the other hand, SMNs with a reduced number of microhooks (Type V, larger microhook axial spacing) demonstrated slightly decreased penetration force (0.3 mN), similar pull-out force (30 mN), and even higher PPR ($\sim$100). Overall, these investigations determined that a smaller microhook base diameter and lower pattern density are beneficial for low penetration force, while microneedle stiffness increases the required pull-out force for more robust anchoring.

The results suggest that appropriate mechanical stiffness plays an essential role in better tissue anchoring (pull-out), while surface microhook dimensions and pattern density primarily influence tissue penetration.

IV. Conclusion

Overall, this work successfully demonstrated a hybrid, passive tissue-anchoring prototype for compact ingestible system integration for prolonged GI interventions. The above characterizations confirm the reliability of the SMU for effective spring compression with a dissolvable polymer and passive actuation. Future works include demonstrating pH-sensitive polymer dissolution for targeted SMU actuation, PEG dissolution and tissue anchoring with the SMU array in a benchtop setting, as well as a test on the dummy capsule that utilizes the SMU package in an *in vitro* model of a GI tract.

Acknowledgment

The authors would like to acknowledge Terrapin Works, as well as Maryland Nanocenter and its FabLab at University of Maryland, College Park, for their support in fabrication and characterization.

References

[1] C. Steiger, A. Abramson, P. Nadeau, A. P. Chandrakasan, R. Langer, and G. Traverso, "Ingestible electronics for diagnostics and therapy," *Nature Rev. Mater.*, vol. 4, no. 2, pp. 83–98, Feb. 2019, doi: 10.1038/s41578-018-0070-3.

[2] C. V. Almario, M. L. Ballal, W. D. Chey, C. Nordstrom, D. Khanna, and B. M. R. R. Spiegel, "Burden of gastrointestinal symptoms in the United States: Results of a nationally representative survey of over 71,000 Americans," *Am. J. Gastroenterol.*, vol. 113, no. 11, pp. 1701–1710, 2018, doi: 10.1038/s41395-018-0256-8.

[3] A. Abramson *et al.*, "A luminal unfolding microneedle injector for oral delivery of macromolecules," *Nature Med.*, vol. 25, no. 10, pp. 1512–1518, Oct. 2019, doi: 10.1038/s41591-019-0598-9.

[4] V. Pensabene, P. Valdastri, S. Tognarelli, A. Menciassi, A. Arezzo, and P. Dario, "Mucoadhesive film for anchoring assistive surgical instruments in endoscopic surgery: *In vivo* assessment of deployment and attachment," *Surgical Endoscopy*, vol. 25, no. 9, pp. 3071–3079, Sep. 2011.

[5] W. Xie *et al.*, "Design and validation of a biosensor implantation capsule robot," *J. Biomech. Eng.*, vol. 139, no. 8, Aug. 2017, Art. no. 081003.

[6] S. Y. Yang *et al.*, "A bio-inspired swellable microneedle adhesive for mechanical interlocking with tissue," *Nature Commun.*, vol. 4, no. 1, p. 1702, Jun. 2013.

[7] W. K. Cho *et al.*, "Microstructured barbs on the north American porcupine quill enable easy tissue penetration and difficult removal," *Proc. Nat. Acad. Sci. USA*, vol. 109, no. 52, pp. 21289–21294, Dec. 2012, doi: 10.1073/pnas.1216441109.

[8] Z. Chen *et al.*, "Additive manufacturing of honeybee-inspired microneedle for easy skin insertion and difficult removal," *ACS Appl. Mater. Interface*, vol. 10, no. 35, pp. 29338–29346, Sep. 2018, doi: 10.1021/acsami.8b09563.

[9] L.-G. Tran, T.-Q. Nguyen, and W.-T. Park, "Bio-inspired barbed microneedle for skin adhesion with interlocking mechanics," in *Proc. IEEE 32nd Int. Conf. Micro Electro Mech. Syst. (MEMS)*, Jan. 2019, pp. 547–550, doi: 10.1109/MEMSYS.2019.8870874.

[10] D. Han *et al.*, "4D printing of a bioinspired microneedle array with backward-facing barbs for enhanced tissue adhesion," *Adv. Funct. Mater.*, vol. 30, no. 11, Mar. 2020, Art. no. 1909197, doi: 10.1002/adfm.201909197.

[11] S. Liu, S. Chu, G. E. Banis, L. A. Beardslee, and R. Ghodssi, "Biomimetic barbed microneedles for highly robust tissue anchoring," in *Proc. IEEE 33rd Int. Conf. Micro Electro Mech. Syst. (MEMS)*, Vancouver, BC, Canada, Jan. 2020, pp. 885–888.

Authorized licensed use limited to: University of Maryland College Park. Downloaded on June 14,2020 at 13:06:24 UTC from IEEE Xplore. Restrictions apply.

This article has been accepted for inclusion in a future issue of this journal. Content is final as presented, with the exception of pagination.

[12] R. A. Hammond, "The proboscis mechanism of *Acanthocephalus ranae*," *J. Express Biol.*, vol. 45, no. 2, pp. 203–213, 1966.
[13] M. Paredes and E. Rodrigue, "Optimal design of conical springs," *Eng. Comput.*, vol. 25, no 2, 2009, Art. no. 147.
[14] E. D. Lemma *et al.*, "Mechanical properties tunability of three-dimensional polymeric structures in two-photon lithography," *IEEE Trans. Nanotechnol.*, vol. 16, no. 1, pp. 23–31, Jan. 2017, doi: 10.1109/TNANO.2016.2625820.
[15] S. Rodríguez and A. Frölich, "3D micro-printing goes macro: Tailor-made materials enable pioneering developments and applications," *Laser Technik J.*, vol. 14, no. 5, pp. 31–33, Nov. 2017.
[16] N. Bolourchian, M. M. Mahboobia, and S. Dadashzadeh, "The effect of PEG molecular weights on dissolution behavior of Simvastatin in solid dispersions," *Iranian J. Pharmaceutical Res.*, vol. 12, no. Suppl, p. 11, 2013.
[17] G. E. Banis, L. A. Beadslee, J. M. Stine, R. M. Sathyam, and R. Ghodssi, "Gastrointestinal targeted sampling and sensing via embedded packaging of integrated capsule system," *J. Microelectromech. Syst.*, vol. 28, no. 2, pp. 219–225, Apr. 2019.
[18] P. Li, C. Kreikemeier-Bower, W. Xie, V. Kothari, and B. S. Terry, "Design of a wireless medical capsule for measuring the contact pressure between a capsule and the small intestine," *J. Biomech. Eng.*, vol. 139, no. 5, p. 51003, May 2017.

Sanwei Liu received the B.S. degree in mechanical engineering from Central South University, Changsha, China, in 2010, and the Ph.D. degree in mechanical engineering from Northeastern University, Boston, MA, USA, in 2018, under the supervision of Prof. C. Livermore. His research focuses on characterizing and engineering marcroscale carbon nanotube networks using electrically induced graphitization for developing high-performance fibers with exceptional mechanical, electrical, and thermal properties. He has been a Post-Doctoral Associate with the MEMS Sensors and Actuators Laboratory (MSAL), University of Maryland, College Park, MD, USA, since 2018. His research focuses on developing robust tissue anchoring structures to enable ingestible devices for long term functionalities in the gastrointestinal tract.

Sangwook Chu (Member, IEEE) received the B.S. degree in electrical and computer engineering from Hanyang University, Seoul, South Korea, in 2012, and the Ph.D. degree in electrical and computer engineering from the University of Maryland, College Park, MD, USA, in August 2018.

His thesis research has focused on developing biofabrication technology using genetically-engineered Tobacco mosaic virus for developing miniature biochemical sensors and energy storage/harvesting devices that rely on electrochemical transduction. He is currently a Post-Doctoral Associate with the Institute for Systems Research, University of Maryland. He is also strongly interested in design, fabrication, and implementation of 3-D micro/nano structured materials for advancing a wide range of research areas, including energy storage/harvesting and biomedical devices.

Luke A. Beardslee received the B.S. and M.Eng. degrees in electrical engineering from Cornell University, Ithaca, NY, USA, in 2007, the Ph.D. degree in electrical engineering from the Georgia Institute of Technology, Atlanta, GA, USA, in 2011, and the M.D. degree from Albany Medical College, Albany, NY, USA, in 2015. He completed a General Surgery Internship at the Walter Reed National Military Medical Center, Bethesda, MD, USA, in 2016. He has held several research positions including a Research Scientist at the State University of New York Institute of Technology Center for Nanoscale Science and Engineering, Albany, NY, USA, and a Visiting Scholar with the Institute for Systems Research, University of Maryland College Park, College Park, MD, USA. His research interests include micro/nanofabrication techniques, transducer development, and ingestible, implantable, and wearable sensing systems.

Reza Ghodssi (Fellow, IEEE) was the Director of the Institute for Systems Research (ISR) from 2009 to 2017. During this time, he launched a number of interdisciplinary initiatives, such as the Maryland Robotics Center and the Brain and Behavior Initiative, aimed at enhancing the impact of ISR research efforts on society while building a more interactive faculty, staff, and student community across different disciplines in the institute. He is currently the Herbert Rabin Distinguished Chair of engineering and the Director of the MEMS Sensors and Actuators Laboratory, Department of Electrical and Computer Engineering, and ISR, University of Maryland, where he is also a Distinguished Scholar–Teacher. He is the Co-Editor of the MEMS Materials and Processes Handbook published in 2011. He holds eight U.S. patents, with another seven pending. His research interests are in the design and development of micro/nano/bio devices and systems for chemical and biological sensing, small-scale energy conversion, and harvesting with a strong emphasis toward healthcare applications. He is a fellow of AVS and ASME. He is an Associate Editor of the *Journal of Microelectromechanical Systems* and *Biomedical Microdevices*.

Authorized licensed use limited to: University of Maryland College Park. Downloaded on June 14,2020 at 13:06:24 UTC from IEEE Xplore. Restrictions apply.